Space-Time Ambiguity Function in 3-D ISR

John Swoboda,[1] Joshua Semeter,[1] Philip Erickson[2]

———

Corresponding author: J. P. Swoboda, Department of Electrical & Computer Engineering, Boston University, 8 Saint Marys Street Boston, MA 02215, USA. (swoboj@bu.edu)

[1]Department of Electrical & Computer Engineering, Boston University, Boston, Massachusetts, USA.

[2]Atmospheric Science Division, MIT Haystack Observatory, Westford Massachusetts, USA.

By leveraging electronically steerable phased array antenna technology, incoherent scatter radars (ISR) have now become full three-dimensional remote sensors for ionosphere plasmas. Currently these systems are operating in the high latitude region where the ionosphere is highly dynamic in both space and time. Because of the highly dynamic nature of the ionosphere in this region it is import to differentiate between artifacts and the true behavior of the plasma. Often the three dimension data is fitted in a spherical coordinate space and then the parameters are interpolated to a Cartesian grid. This and other sources of error could be impacting the reconstructions of the plasma parameters.

In this study we present a new way of analyzing 3-D dimension ISR through use of the space-time ambiguity function. This concept is similar to the range ambiguity function that is used in traditional ISR for scanning antenna systems but has been extended to all spatial dimension along with time as well.

The use of this new ambiguity function allow us to pose this problem in terms of a linear inverse problem for the lags of the intrinsic plasma autocorrelation function. From this we can explore the impact of non-stationarity in the plasma parameters in both time and space. Along with showing possible artifacts we will begin to explore ways of reducing these artifacts.

1. Introduction

Incoherent scatter radar (ISR) systems have enabled researchers since the 1950's to explore the ionosphere [*Gordon*, 1958]. Using methodology developed by Dougherty, Farley and others these systems can give measurements of electron density N_e, Ion temperature T_i, electron temperature T_e, Ion velocity V_i and other plasma parameters [*Dougherty and Farley*, 1960; *Farley et al.*, 1961; *Dougherty and Farley*, 1963; *Hagfors*, 1961]. These parameters are measured by fitting a nonlinear theoretic autocorrelation function (ACF) model derived from first principles physics to an estimated intrapulse time autocorrelation of the scattered radar signal [*Lehtinen and Huuskonen*, 1996].

As with any real world measurement method there is limit to the spatial and temporal resolution of ISR systems. This resolution is determined by the ability of the sensor to create independent measurements of the ACF in time and space of what is essentially a zero-mean complex Gaussian process. At space and time extents smaller then these resolutions the random process that the ACF is derived from is assumed to be stationary. In ISR literature the ambiguity function encapsulates the spatial resolution in the range dimension. This ambiguity emerges as a function of range and correlation lag due to the pulse modulation and the finite bandwidth of the receiver [*Farley*, 1969]. The time resolution is determined by how long it takes to average the autocorrelation function to reduce the variance of the estimate to a desired level.

41 This assumption of stationarity at the level of the ambiguity function constrains the

42 measurement and creates a blurring and other forms of artifacts due to the non-linear

43 fitting of plasma parameters. In order to reduce the impact of these ambiguities a

44 number techniques have been developed. Some techniques include trying to reduce

45 the extent of the ambiguity function by adjusting the waveform. Barker code wave

46 forms are used in ISR but mainly for low altitude studies of the E-region due to the

47 inability to form a spectrum from them. Another method for reducing the ambiguity

48 in range is using alternating codes [*Gray and Farley*, 1973; *Lehtinen and Haggstrom*,

49 1987; *Sulzer*, 1993; *Sulzer*, 1989].

50 Another set of techniques often shown in the literature focus on reducing the impact

51 of the ambiguity function through post processing. The first method, full profile

52 analysis, consists of fitting physical parameter values to entire range extent taking

53 into account all of the correlations between all locations [*Holt et al.*, 1992; *Lehtinen*,

54 1989; *Lehtinen et al.*, 1997; *Hysell et al.*, 2008]. This technique often places constraints

55 on the physical parameters as in *Hysell et al.* [2008]. Because the the relationship

56 between the autocorrelation function and the lags are non-linear this method often

57 yields algorithms that require a large amount computation to calculate the covariance

58 matrices between all of the values.

59 The other set of post processing methods, such as in *Nikoukar et al.* [2008] and

60 *Virtanen et al.* [2008], treat the problem as a linear inverse problem of the lags.

61 Methods such as total-variations or Tikihonov regularization can be applied to the

62 lags to try to fill in the missing information nation from the null space of the operator.

63 These methods are easy to compute and can rely on a large body of knowledge from

64 engineering communities that study linear inverse problems.

65 Recently phased array technology has started to be leveraged by ISR community.

66 The Advance Modular Incoherent Scatter Radar (AMISR) systems have already been

67 deployed both at the Poker Flat Alaska (PFISR) and Resolute Bay Canada (RISR)

68 [ami, 2014]. The EISCAT-3D project is currently being developed using phased array

69 technology as well and will be capable of multistatic processing [eis, 2005]. These

70 new systems are already being used to create three dimensional reconstructions of

71 plasma parameters [*Semeter et al.*, 2009], [*Nicolls and Heinselman*, 2007; *Dahlgren*

72 *et al.*, 2012a, b].

73 There has been no formal derivation of an ambiguity function for all three spatial

74 dimensions for these systems, although up until recently ISR systems, which only

75 had dish antennas, could not mitigate the finite beam width effects. In a highly

76 dynamic region like the high latitude ionosphere this lack of knowledge can be prob-

77 lematic. There are numerous phenomena such as polar cap patches that may be

78 moving through the field of view at very high speeds [*Dahlgren et al.*, 2012a]. This

79 motion can cause an apparent expansion in the shape of the beams if one represents

80 the beams in the frame of reference of the moving plasma.

81 These three-dimensional reconstructions often consist of taking the fitted param-

82 eters and then interpolating them to a Cartesian space from the system's natural

83 spherical coordinate space [*Butler*, 2013]. The step of fitting the autocorrelation

84 function to the theoretical functions to find the final plasma parameters is a non-

85 linear operation. Because of this it is impossible to exactly predict the impact on the

86 parameter values as different plasma populations move through the field of view of

87 the radar. Alternatively it is possible to treat the formation of the autocorrelation

88 estimates as a linear process with each lag as an independent channel [*Nikoukar et al.*,

89 2008].

90   Using this methodology we can make many parallels between ISR and CCD cam-

91 eras. In cameras bluring can take place when an object moves over a space covered

92 by one pixel while the shutter is open and the CCD is collecting photons. A diagram

93 of this can be seen in Figure 1. The same holds for ISR except that the pixels are no

94 longer square and instead are determined by the beam shape and pulse pulse pattern.

95 This is shown in the diagrams in Figure 2.

96   In this publication we will develop a model for a full three dimensional space-time

97 ambiguity function for 3-D ISR systems. This function can also be modified to show

98 the ambiguity within the rest frame of the moving plasma. In the end this full three

99 dimensional can be represented as kernel in a Fredholm integral equation like in

100 Equation 1 with $f(s)$ being the lag of the autocorrelation function at a specific time

101 and position.

$$g(t) = \int_a^b K(t,s)f(s)ds \tag{1}$$

102   The impact of the three-dimensional ambiguity on moving plasma will be shown

103 through simulation. This ISR simulator fully emulates the ISR data creation process

104 at the IQ level.

105 Lastly possible mitigation techniques will be explored. These mitigation techniques

106 will borrow heavily from the image and signal processing literature.

2. Space-Time Ambiguity

107 The three dimensional nature of the problem requires first defining the spatial

108 coordinate system, $\mathbf{r} = [x, y, z]^T$. For this coordinate system, $\mathbf{r} = [0, 0, 0]^T$ at the

109 location of the radar and thus $r = |\mathbf{r}|$, also known as the range variable. This allows

110 for the use of polar coordinates $\mathbf{r} = [r, \theta, \phi]^T$ where θ is the physical elevation angle,

111 ϕ is the physical azimuth angle.

112 The radar will sample this space into a set of discrete points which will be referred

113 to as $\mathbf{r}_s = [x_s, y_s, z_s]^T$ along with the descritized range $r_s = |\mathbf{r}_s|$. The sampled space

114 will consist of a number of points which are the combinations of the range gates

115 and number of beams. This points can also be referred in the polar coordinates

116 $\mathbf{r}_s = [r_s, \theta_s, \phi_s]^T$, where θ_s is the sampled elevation angle, ϕ_s is the sampled azimuth

117 angle.

118 For notation purposes we use two different sets of time commonly known in radar

119 literature as fast-time, n and slow-time, t [*Richards*, 2005].. Fast-time is used to

120 explore the workings of the radar on the order of the radar systems A/D conversion

121 such as lag formation. Slow-time will used for processes that vary in time on the

122 order of the system's pulse repetition interval (PRI). In order to form estimates of

123 the ACFs it is assumed that the plasma parameters parameters will change on the

124 order of 10 to hundreds of PRIs. The term n will be a sampled parameter while t

125 will represent a continuous time and t_s will be the slow time parameter sampled by

126 the radar.

2.1. Derivation

127   The basic physical mechanism behind ISR is that electron density fluctuations in

128 the ionosphere, $n_e(\mathbf{r}, n)$, scatter radio waves which can be observed by the receiver

129 system of the radar [*Hysell et al.*, 2008]. The emitted radar signal will have a pulse

130 shape $s(n)$ modulated at a central frequency that results in a scattering wave num-

131 ber $\mathbf{k}$. Using the Borne approximation the signal received at time n, $x(n)$, can be

132 represented as the following

$$x(n) = h(n) * \int_{\mathbf{r}} e^{-j\mathbf{k}\cdot\mathbf{r}} s\left(n - \frac{2r}{c}\right) n_e(\mathbf{r}, n)d\mathbf{r}, \tag{2}$$

133 where $h(n)$ is the receiver filter. Generally it is assumed that the pass band of the

134 filter is larger then the bandwidth of the electron density fluctuation [*Kudeki*, 2003].

135 As such it can be assumed that filter will only act on the the shape of the pulse. This

136 will change Equation 2 to the following:

$$x(n) = \int_{\mathbf{r}} e^{-j\mathbf{k}\cdot\mathbf{r}} a\left(n - \frac{2r}{c}\right) n_e(\mathbf{r}, n)d\mathbf{r} \tag{3}$$

137 where $a(n) = h(n) * s(n)$.

138   When the autocorrelation of the signal is done we find the following formula,

139 [*Nikoukar et al.*, 2008],

$$\langle x(n)x^*(n')\rangle = \int_{\mathbf{r}'}\int_{\mathbf{r}} e^{-2j\mathbf{k}\cdot(\mathbf{r}'-\mathbf{r})} a\left(n - \frac{2r}{c}\right) a^*\left(n + \tau - \frac{2r'}{c}\right)\langle n_e(\mathbf{r},n)n_e^*(\mathbf{r}',n')\rangle d\mathbf{r}d\mathbf{r}'$$

(4)

where r' is the magnitude of the vector $\mathbf{r}'$. If we assume stationarity of the second order statistic of the signal along fast time n we can substitute a lag variable $\tau \equiv n' - n$, Equation 4 becomes

$$\langle x(n)x^*(n+\tau)\rangle = \int_{\mathbf{r}'}\int_{\mathbf{r}} e^{-2j\mathbf{k}\cdot(\mathbf{r}'-\mathbf{r})} a\left(n - \frac{2r}{c}\right) a^*\left(n + \tau - \frac{2r'}{c}\right)\langle n_e(\mathbf{r},n)n_e^*(\mathbf{r}',n+\tau)\rangle d\mathbf{r}d\mathbf{r}'.$$

(5)

We can make a simplifying assumption at this point that the space-time autocorrelation function of $n_e(\mathbf{r},t)$, $\langle n_e(\mathbf{r},n)n_e(\mathbf{r}',n+\tau)\rangle$, will go to zero as the magnitude of $\mathbf{x} \equiv \mathbf{r}' - \mathbf{r}$ increases. The rate that the space-time autocorrelation goes to zero will be such that $\tau \gg ||\mathbf{x}||$ thus in the argument of the pulse shape $r \approx r'$. This allows Equation 5 to be rewritten as

$$\langle x(n)x^*(n+\tau)\rangle = \int_{\mathbf{r}} a\left(n - \frac{2r}{c}\right) a^*\left(n + \tau - \frac{2r}{c}\right) \int_{\mathbf{x}} e^{-2j\mathbf{k}\cdot\mathbf{x}}\langle n_e(\mathbf{r},n)n_e^*(\mathbf{x}+\mathbf{r},n+\tau)\rangle d\mathbf{x}d\mathbf{r}.$$

(6)

The inner integral is a spatial Fourier transform evaluated at the wave number of the radar $\mathbf{k}$

$$\langle |n_e(\mathbf{k},r,\tau)|^2\rangle \equiv \int_{\mathbf{x}} e^{-2j\mathbf{k}\cdot\mathbf{x}}\langle n_e(\mathbf{r},b)n_e^*(\mathbf{x}+\mathbf{r},n+\tau)\rangle d\mathbf{x}.$$

(7)

Now Equation 6 becomes

$$\langle x(n)x^*(n+\tau)\rangle = \int_r a(n - \frac{2r}{c})a^*(n+\tau - \frac{2r}{c})\langle|n_e(\tau,\mathbf{k},\mathbf{r})|^2\rangle dr. \tag{8}$$

If n is replaced with $2r_s/c$ we can introduce the range ambiguity function $W(\tau, r_s, r)$ by doing the following substitution [*Nikoukar*, 2010],

$$W(\tau, r_s, r) = a\left(\frac{2(r_s - r)}{c}\right) a^* \left(\frac{2(r' - r)}{c} + \tau\right). \tag{9}$$

149   In order to simplify notation we will represent $\langle|n_e(\tau,\mathbf{k},\mathbf{r})|^2\rangle$, as $R(\tau, \mathbf{r})$. Assuming,

150 for the moment, that R only varies across the range dimension r we can now represent

151 this in the form of a Fredholm integral equation

$$\langle x(2r_s/c)x^*(2r_s/c + \tau)\rangle = \int_r W(\tau, r_s, r)R(\tau, r)dr. \tag{10}$$

152 The ambiguity in the end $W(\tau, r_s, r)$ is a lag dependent smoothing along the range

153 dimension of $R(\tau, r)$.

The spatial ambiguity across angle is determined by the antenna beam pattern. In phase array radars this beam pattern is ideally the array factor multiplied by the element pattern [*Balanis*, 2005]. The array factor is determined by a number of things including the element spacing in both x and y (dx, dy) and the wave number of the radar, k. Making idealized assumptions with no mutual coupling and that the array elements are cross dipole elements AMISR systems will have the following antenna pattern for pointing angle (θ_s, ϕ_s),

$$F(\theta_s, \phi_s, \theta, \phi) = \frac{1}{2}(1 + \cos(\theta)^2)\left[\frac{1}{MN}\left(1 + e^{j(\psi_y/2 + \psi_x)}\right)\frac{\sin((M/2)\psi_x)}{\sin(\psi_x)}\frac{\sin((N/2)\psi_x)}{\sin(\psi_x/2)}\right]^2,$$
$$\tag{11}$$

where $\psi_x = -kd_x(\sin\theta\cos\phi - \sin\theta_s\cos\phi_s)$, $\psi_y = -kd_y(\sin\theta\sin\phi - \sin\theta_s\sin\phi_s)$ and

M is the number of elements in the x direction of the array N is the number of

elements in the y direction(see Appendix: A for derivation).

This spatial ambiguity is a separable function made up of the components of $W(\tau, r)$

and $F(\theta_s, \phi_s, \theta, \phi)$. These two functions can be combined by multiplying the two, cre-

ating the spatial ambiguity function $K(\tau, \mathbf{r}_s, \mathbf{r})$, and then doing a volume integration.

This will create radar system's estimate of the ACF with one pulse which will be re-

ferred to as $\rho(\tau, \mathbf{r}_s)$,

$$\rho(\tau, \mathbf{r}_s) = \int F(\theta_s, \phi_s, \theta, \phi)W(\tau, r_s, r)R(\tau, \mathbf{r})dV, \tag{12}$$

$$= \int K(\tau, \mathbf{r}_s, \mathbf{r})R(\tau, \mathbf{r})dV. \tag{13}$$

A rendering of an example of this full ambiguity function for an uncoded long pulse

and antenna pattern in Equation 11 for four beams can be seen in Figure 3.

This one pulse is a single sample of a random process. In order to create a usable

estimate of the ACF numerous instances of this ACF need to be averaged together

to reduce the variance in order to fit the estimate to a theoretical ACF that is tied

to specific parameter values.

Lastly, since the radar requires a finite amount of time to average pulses to create

the estimate of the ACF we will add slow-time dependence to R. We will add another

separable function $G(t_s, t)$ to the kernel,

$$\rho(\tau, \mathbf{r}_s, t_s) = \int G(t_s, t) K(\tau, \mathbf{r}_s, \mathbf{r}) R(\tau, \mathbf{r}, t) dV dt \tag{14}$$

$$\rho(\tau, \mathbf{r}_s, t_s) = \int L(\tau, \mathbf{r}_s, t_s, \mathbf{r}, t) R(\tau, \mathbf{r}, t) dV dt. \tag{15}$$

171 The final kernel, $L(\tau, \mathbf{r}_s, t_s, \mathbf{r}, t)$ encompasses the full space-time ambiguity.

2.2. Ambiguity after Frame Transformation

172   We will now focus on the impact of the motion of plasma as it is going through the

173 field of view of the radar. We will assume that the radar is integrating over a length

174 of time T beginning at t_s. The kernel L will be represented as a separable function

175 K and G as in Equation 14. In this case G will be an indicator function of length T

176 and centered at $t_0 + 1/2$. This will change Equation 14 to the following,

$$\rho(\tau, \mathbf{r}_s, t_s) = \int K(\tau, \mathbf{r}_s, \mathbf{r}) \int_{t_s}^{t_s+T} R(\tau, \mathbf{r}, t) dt dV. \tag{16}$$

177   Of specific interest are instances in the high latitude ionosphere where embedded

178 plasma structures are moving due to the electric field of the magnetosphere. Because

179 of this it will be assumed that the plasma is rigid object and will not deform with

180 respect to $\mathbf{r}$ over time period $[t_0, t_0 + T]$. Also it will be assumed that it will be

181 moving with a constant velocity $\mathbf{v}$. Thus $R(\tau, \mathbf{r}, t) \Rightarrow R(\tau, \mathbf{r} + \mathbf{v}t)$. At this point

182 Equation 16 becomes,

$$\rho(\tau, \mathbf{r}_s, t_s) = \int \int_{t_s}^{t_s+T} K(\tau, \mathbf{r}_s, \mathbf{r}) R(\tau, \mathbf{r} + \mathbf{v}t) dt dV \tag{17}$$

A change of variables where $\mathbf{r}' = \mathbf{r} + \mathbf{v}t$ acts as a Galilean transform and applies a warping to the kernel and changing the frame of reference. Then Equation 17 becomes

$$\rho(\tau, \mathbf{r}_s, t_s) = \int \int_{t_s}^{t_s+T} K(\tau, \mathbf{r}_s, \mathbf{r}' - \mathbf{v}t)R(\tau, \mathbf{r}')dt dV. \tag{18}$$

Since $R(\tau, \mathbf{r}')$ is no longer dependent on t Equation18 becomes,

$$\rho(\tau, \mathbf{r}_s, t_s) = \int \left[\int_{t_s}^{t_s+T} K(\tau, \mathbf{r}_s, \mathbf{r}' - \mathbf{v}t)dt \right] R(\tau, \mathbf{r}')dV. \tag{19}$$

By performing the integration in t the problem can now be simplified further back to a Fredholm integral equation by simply replacing the terms in the square brackets as a new kernel A,

$$\rho(\tau, \mathbf{r}_s, t_s) = \int A(\tau, \mathbf{r}_s, t_s, \mathbf{r}')R(\tau, \mathbf{r}')dV. \tag{20}$$

The impact of the plasma velocity on the ambiguity function can be seen in Figure 4. This is the same ambiguity as seen in Figure 3 but with a velocity of 500 m/s in the y direction over a period of 2 minutes. This velocity creates a larger ambiguity function in the frame of reference of the moving plasma.

The operator A can be determined through knowledge of the radar system's beam pattern along with the experiments pulse pattern, integration time and velocity of the plasma. This velocity $\mathbf{v}$ can be estimated by taking measurements of the Doppler shift and using a methodology seen in [*Butler et al.*, 2010]. Once the operator has

198 been determined standard processing techniques can be used as if the plasma is not

199 moving.

3. Simulation

200   In order to show the impact of the ambiguity function, synthetic data was created

201 using a known condition of a simulated ionosphere. The simulator creates data by

202 deriving filters from the autocorrelation function and applying it to complex white

203 Gaussian noise. In a sense every point in time and space noise plant and filter

204 structure as in Figure 5. The data is then scaled and summed together according to

205 its location in range and angle space to radar.

206   After the IQ data has been created it is processed in to create an estimates of the

207 ACF at desired points of space. This processing follows flow chart seen in Figure 6.

208   The sampled I/Q can be represented as $x(n) \in \mathbb{C}^N$ where N is the number of

209 samples in an inter pulse period. At this point the first step in estimating the auto-

210 correlation function is taken. For each range gate $m \in 0, 1, ... M-1$ an autocorrelation

211 is estimated for each lag of $l \in 0, 1..., L-1$. To get better statistics this operation is

212 performed for each pulse $j \in 0, 1, ... J-1$ and then summed over the J pulses. The

213 entire operation to form the initial estimate of $\hat{R}(m,l)$ can be seen in Equation 21:

$$\hat{R}(m,l) = \sum_{j=0}^{J-1} x(m - \lfloor l/2 \rfloor, j)x^*(m + \lceil l/2 \rceil, j). \tag{21}$$

214   The case shown in Equation 21 is a centered lag product, other types of lag products

215 calculations are available but generally a centered product is used. In the centered lag

216 product case range gate index m and sample index n can be related by $m = n - \lfloor L/2 \rfloor$

217 and the maximum lag and sample relation is $M = N - \lceil L/2 \rceil$.

218   After the lag products have been formed an estimate of the noise correlation is

219 subtracted out of $\hat{R}(m, l)$, which is defined as $\hat{R}_w(m, l)$:

$$\hat{R}_w(m_w, l) = \sum_{j=0}^{J-1} w(m_w - \lfloor l/2 \rfloor, j) w^*(m_w + \lceil l/2 \rceil, j), \qquad (22)$$

220 where $w(n_w)$ is the background noise process of the radar. Often the noise process

221 is sampled during a calibration period for the radar when nothing is being emitted.

222 The final estimate of the autocorrelation function after the noise subtraction and

223 summation rule will be represented by $\hat{R}_f(m, l)$. At this point a summation rule is

224 applied and the data is sent off to be fit.

225   In order to demonstrate the blurring taking place from the motion of plasma a

226 phantom ionosphere is created where a small plasma enhancement moves through

227 the radar field of view. The background electron density varies in altitude as a

228 Chapman function while the electron and ion temperature remains constant. This

229 can be seen in Figure 7. This is done to avoid having to do full fit and thus only try

230 to measure the electron density. Also estimates of the zeroth lag are only necessary.

231 Added to this is a 35 km radius sphere of enhance electron density of about 5×10^{10}

232 m^{-3} centered at 400 km altitude moving at 500 m/s along the $\mathbf{y}$ direction. Images

233 from this phantom can be seen in Figure 8.

234   Using the phantom we can see how just simply changing the integration time can

235 impact the reconstruction. In Figure 10 we can see a case were only 10 pulses are used

²³⁶ for the reconstruction. This corresponds to an integration time of about 9 seconds

²³⁷ using the 121 beam pattern which can be seen in Figure 9. The enhancement can be

²³⁸ seen with concentrated energy as it moves through the field of view. The problem

²³⁹ is that there is a high amount of variance in the reconstruction. Figure 11 shows

²⁴⁰ the reconstruction with 200 pulses, 3 minute integration time. The variability has

²⁴¹ been reduced but there is a large amount of blurring of the enhancement as it moves

²⁴² through the field of view.

²⁴³ In order to give a comparison a phantom was also created with no motion. This

²⁴⁴ can be seen in first pane Figure 12. An image using the same integration time as

²⁴⁵ in Figure 10 for the stationary phantom is the center pane in Figure 12. Another

²⁴⁶ image using the longer integration time can be seen in right pane of Figure 12. These

²⁴⁷ images show that the blurring is on the same order between both integration times.

²⁴⁸ Lastly we show results of a simulation of the plasma density enhancement through

²⁴⁹ the field of view with full fitting. We again use a plasma enhancement moving through

²⁵⁰ the field of view at 500 m/s but the electron and ion tempreture varies with time and

²⁵¹ altitude. The the background ion and electron temperature vs. height can be seen

²⁵² in Figure 14. As the electron density enhancement travels through the field of view

²⁵³ the temperatures drop by the same ratio that the electron density is enhanced.

²⁵⁴ The phantoms for each parameter at approximately 402 seconds can be seen in

²⁵⁵ Figure 14. The reconstruction of this field at the same time can be seen in Figure 15.

²⁵⁶ The reconstruction does not seem to show the electron density enhancement even in

²⁵⁷ a blurred form. This is likely due to the nonlinear nature of the fitting.

4. Possible Mitigation Techniques

There are a number of possible ways to remove the ISR operator function to the data. A relatively simply way to remove the problem is to process the data in the frame of reference of the plasma. This technique includes measuring the ion velocity of the plasma and then integrating the beams that the plasma is present in as it moves through the field of view.

In order to reconstruct the plasma parameters it is necessary to do some sort of regularization. There are two type of regularization that can be applied in this case the first is parameter based regularization, like full profile analysis, and the other is data based regularization. The term parameter based regularization in this case means applying constraints to the physical parameters that are often determined after fitting. This requires a large amount of calculation because the fitting and constraints are done in one step. Currently full profile analysis has only been applied along the range dimension and not in all three spatial dimensions. Extending this to three dimensions may make these algorithms computationally infeasible.

Data based regularization infers the application of constraints to the estimates of the autocorrelation functions. The constraints usually deal with how the data changes over time and space by constraining the energy of the ACFs or its derivative. This has an advantage of being more computationally tractable in that it is now a linear inverse problem. Using the ideas stated in this paper one can cast the reconstruction of the four dimensional function of the ACFs in these terms. The issue with doing

278 this data based reconstruction is it is unknown how to constrain the reconstruction

279 in the best way.

280   The two examples of data based regularization in the one dimensions ISR literature

281 are lag profile inversion and deconvolution methods. Lag profile inversion creates an

282 operator that takes the measured data from a theoretical ACFs to the measured ACFs

283 [*Virtanen et al.*, 2008]. Along with the operator there is also an assumed Gaussian

284 error. This error can be then estimated from the data. This Bayesian frame work can

285 actually be rewritten as a least squares minimization along with a Tikinov constraint.

286 Because of this one can show that the deconvolution methods from *Nikoukar et al.*

287 [2008] have almost the same structure as lag profile inversion.

288   With this in mind one can go a step further and investigate super resolution meth-

289 ods seen in image processing literature [*Takeda et al.*, 2009],[*Takeda and Milanfar*,

290 2011]. With these techniques along with the data regularization based frame work

291 in one dimensional ISR these techniques could be used to reconstruct the ACFs.

292 This would require a complete change in the methodology in which 3-D ISR data is

293 investigated. Basically instead of fitting data in the coordinate space of the radar

294 we would first re-grid the data in a Cartesian space and then apply the nonlinear

295 fitting. This would have the advantage of working with a linear inverse problem but

296 the issues would be the same as with other data based regularization techniques were

297 there is a question of what type of constraint should be used as opposed to a straight

298 forward physical constraint.

5. Conclusion

We have presented a new method for analyzing incoherent scatter radar processing through use of the full space-time ambiguity function. This allows for taking into account the antenna beam pattern, pulse pattern and time integration. Through simulation we have shown how plasma motion can impact reconstruction of parameters which compounded with the non-linear nature of the parameter fitting step can create errors which are hard to predict. Lastly we have suggested a number of ways using three dimensional ISR systems we could mitigate these errors and reconstruct parameters at higher resolutions then what is currently possible.

Appendix A: Derivation of Idealized AMISR Array Pattern

The current antenna on the AMISR systems is made up 8x16 set of panel of half wave cross dipoles. Each panel has 32 cross dipoles in a 8x4 hexagonal configuration. In the current set up at the Poker Flat site this yields at 4096 element array in a 64x64 element hexagonal configuration.

In order to simplify the antenna can be treated as two rectangular arrays of cross dipoles interleaved together. In the x direction each of these arrays will have a spacing of $2d_x$ with $M/2$ elements. The y direction will be of length N elements and spacing d_y. Using basic planar phase array theory, [*Balanis*, 2005], we can start with the linear array pattern from the first array can be represented as

$$E_1(\theta, \phi) = \sum_{m=1}^{M/2} \sum_{n=1}^{N} e^{-j2(m-1)kd_x \sin\theta\cos\phi - j(n-1)kd_y \sin\theta\sin\phi}. \tag{A1}$$

Since the second array can be though of a shifted version of the first in the x direction

we get the following

$$E_2(\theta, \phi) = \sum_{m=1}^{M/2}\sum_{n=1}^{N} e^{-j(2m-1)kd_x\sin\theta\cos\phi - j(n-1/2)kd_y\sin\theta\sin\phi}. \qquad (A2)$$

In order to simplify notation we will make the following substitutions, $\psi_x =$

$-kd_x\sin\theta\cos\phi$, $\psi_y = -kd_y\sin\theta\sin\phi$. Using Equations A1 and A2 we can see the

following relationship,

$$E_2(\theta, \phi) = e^{j(\psi_y/2 + \psi_x)}E_1(\theta, \phi) = \sum_{m=1}^{M/2}\sum_{n=1}^{N} e^{-j2(m-1)\psi_x - j(n-1)\psi_y}. \qquad (A3)$$

Adding E_1 and E_2 together we get the following linear array pattern

$$\begin{aligned}
E(\theta, \phi) &= \left(1 + e^{j(\psi_y/2 + \psi_x)}\right)\sum_{m=1}^{M/2}\sum_{n=1}^{N} e^{-j2(m-1)\psi_x - j(n-1)\psi_y}. \\
&= \frac{1}{MN}\left(1 + e^{j(\psi_y/2 + \psi_x)}\right)\frac{\sin((M/2)\psi_x)}{\sin(\psi_x)}\frac{\sin((N/2)\psi_x)}{\sin(\psi_x/2)}.
\end{aligned} \qquad (A4)$$

Since the array is steerable this can be taken into account in the equations by

simply changing the definitions of ψ_x and ψ_y to $\psi_x = kd_x(\sin\theta\cos\phi - \sin\theta_s\cos\phi_s)$,

and $\psi_y = kd_y(\sin\theta\sin\phi - \sin\theta_s\sin\phi_s)$. Lastly the antenna pattern of a single cross

dipole can be represented as $\frac{1}{2}(1 + \cos(\theta)^2)$[Balanis, 2005]. By taking the squared

magnitude of the array factor and multiplying it with the pattern of the dipole we

get Equation 11,

$$F(\theta_s, \phi_s, \theta, \phi) = \frac{1}{2}(1 + \cos(\theta)^2) \left| \frac{1}{MN} \left(1 + e^{j(\psi_y/2 + \psi_x)}\right) \frac{\sin((M/2)\psi_x)}{\sin(\psi_x)} \frac{\sin((N/2)\psi_x)}{\sin(\psi_x/2)} \right|^2.$$

(A5)

References

328   (2005), Eiscat 3d design specification document.

329   (2014), Amisr overview.

330   Balanis, C. A. (2005), *Antenna Theory: Analysis and Design*, Wiley-Interscience.

331   Butler, T. W. (2013), Spatial statistics and analysis of Earth's ionosphere, Ph.D.
332   thesis.

333   Butler, T. W., J. Semeter, C. J. Heinselman, and M. J. Nicolls (2010), Imaging f
334   region drifts using monostatic phased-array incoherent scatter radar, *Radio Sci.*,
335   *45*(5), RS5013, doi:10.1029/2010RS004364.

336   Dahlgren, H., J. L. Semeter, K. Hosokawa, M. J. Nicolls, T. W. Butler, M. G. Johnsen,
337   K. Shiokawa, and C. Heinselman (2012a), Direct three-dimensional imaging of polar
338   ionospheric structures with the resolute bay incoherent scatter radar, *Geophysical*
339   *Research Letters*, *39*(5), n/a–n/a, doi:10.1029/2012GL050895.

340   Dahlgren, H., G. W. Perry, J. L. Semeter, J. P. St. Maurice, K. Hosokawa,
341   M. J. Nicolls, M. Greffen, K. Shiokawa, and C. Heinselman (2012b), Space-
342   time variability of polar cap patches: Direct evidence for internal plasma struc-
343   turing, *Journal of Geophysical Research: Space Physics*, *117*(A9), A09,312, doi:
344   10.1029/2012JA017961.

345   Dougherty, J. P., and D. T. Farley (1960), A theory of incoherent scattering of

346   radio waves by a plasma, *Proceedings of the Royal Society of London. Series A,*

347   *Mathematical and Physical Sciences*, *259*(1296), pp. 79–99.

348   Dougherty, J. P., and D. T. Farley (1963), A theory of incoherent scattering of radio

349   waves by a plasma, 3 scattering in a partly ionized gas, *Journal of Geophysical*

350   *Research*, *68*, 5473.

351   Farley, D. T. (1969), Incoherent scatter correlation function measurements, *Radio*

352   *Sci.*, *4*(10), 935–953.

353   Farley, D. T., J. P. Dougherty, and D. W. Barron (1961), A theory of incoherent

354   scattering of radio waves by a plasma ii. scattering in a magnetic field, *Proceedings*

355   *of the Royal Society of London. Series A, Mathematical and Physical Sciences*,

356   *263*(1313), pp. 238–258.

357   Gordon, W. (1958), Incoherent scattering of radio waves by free electrons with appli-

358   cations to space exploration by radar, *Proceedings of the IRE*, *46*(11), 1824–1829,

359   doi:10.1109/JRPROC.1958.286852.

360   Gray, R. W., and D. T. Farley (1973), Theory of incoherent-scatter measurements

361   using compressed pulses, *Radio Sci.*, *8*(2), 123–131, doi:10.1029/RS008i002p00123.

362   Hagfors, T. (1961), Density fluctuations in a plasma in a magnetic field, with ap-

363   plications to the ionosphere, *Journal of Geophysical Research*, *66*(6), 1699–1712,

364   doi:10.1029/JZ066i006p01699.

365   Holt, J. M., D. A. Rhoda, D. Tetenbaum, and A. P. van Eyken (1992), Opti-

366   mal analysis of incoherent scatter radar data, *Radio Sci.*, *27*(3), 435–447, doi:

10.1029/91RS02922.

Hysell, D. L., F. S. Rodrigues, J. L. Chau, and J. D. Huba (2008), Full profile incoherent scatter analysis at jicamarca, *Annales Geophysicae*, *26*(1), 59–75, doi: 10.5194/angeo-26-59-2008.

Kudeki, E. (2003), *ECE 458 Lecture Notes, Application to Radio Wave Propagation*, Univ. Of Illinois, Urbana IL.

Lehtinen, M. S. (1989), On optimization of incoherent scatter measurements, *Advances in Space Research*, *9*(5), 133 – 141, doi:http://dx.doi.org/10.1016/0273-1177(89)90351-7.

Lehtinen, M. S., and I. Haggstrom (1987), A new modulation principle for incoherent scatter measurements, *22*, 625–634, doi:10.1029/RS022i004p00625.

Lehtinen, M. S., and A. Huuskonen (1996), General incoherent scatter analysis and {GUISDAP}, *Journal of Atmospheric and Terrestrial Physics*, *58*(1–4), 435 – 452, doi:http://dx.doi.org/10.1016/0021-9169(95)00047-X, ¡ce:title¿Selected papers from the sixth international Eiscat Workshop¡/ce:title¿.

Lehtinen, M. S., A. Huuskonen, and J. Pirttilä (1997), First experiences of full-profile analysis with GUISDAP, *Annales Geophysicae*.

Nicolls, M. J., and C. J. Heinselman (2007), Three-dimensional measurements of traveling ionospheric disturbances with the Poker Flat Incoherent Scatter Radar, *Geophysical Research Letters*.

Nikoukar, R. (2010), Near-optimal inversion of incoherent scatter radar measurements- coding schemes, processing techniques, and experiments, Ph.D. the-

sis, University of Illinois at Urbana-Champaign.

Nikoukar, R., F. Kamalabadi, E. Kudeki, and M. Sulzer (2008), An efficient near-optimal approach to incoherent scatter radar parameter estimation, *Radio Science*, *43*(5), n/a–n/a, doi:10.1029/2007RS003724.

Richards, M. A. (2005), *Fundamentals of Radar Signal Processing*, McGraw-Hill.

Semeter, J., T. Butler, C. Heinselman, M. Nicolls, J. Kelly, and D. Hampton (2009), Volumetric imaging of the auroral ionosphere: Initial results from pfisr, *Journal of Atmospheric and Solar-Terrestrial Physics*, *71*, 738 – 743, doi: 10.1016/j.jastp.2008.08.014, ¡ce:title¿Advances in high latitude upper atmospheric science with the Poker Flat Incoherent Scatter Radar (PFISR)¡/ce:title¿.

Sulzer, M. P. (1989), Recent incoherent scatter techniques, *Advances in Space Research*, *9*, 153–162, doi:10.1016/0273-1177(89)90353-0.

Sulzer, M. P. (1993), A new type of alternating code for incoherent scatter measurements, *Radio Science*, *28*(6), 995–1001, doi:10.1029/93RS01918.

Takeda, H., and P. Milanfar (2011), Removing Motion Blur With Space-Time Processing, *Image Processing, IEEE Transactions on*, *20*(10), 2990–3000.

Takeda, H., P. Milanfar, M. Protter, and M. Elad (2009), Super-Resolution Without Explicit Subpixel Motion Estimation, *Image Processing, IEEE Transactions on*, *18*(9), 1958–1975.

Virtanen, I. I., M. S. Lehtinen, and T. Nygrén (2008), Lag profile inversion method for EISCAT data analysis, *Annales . . . .*

(a) CCD No Blur   (b) CCD With Blur

Figure 1.   CCD camera

(a) Radar No Blur   (b) Radar With Blur
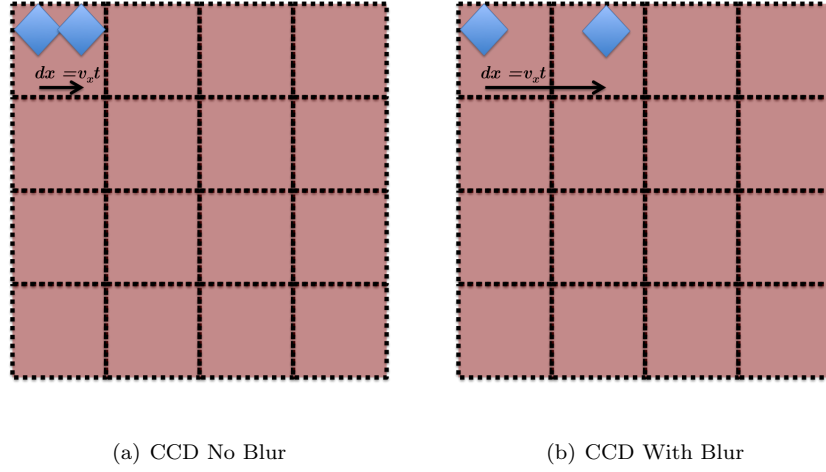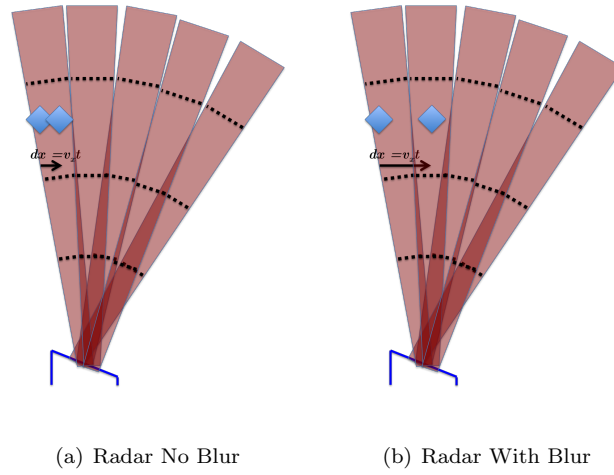
Figure 2.   Radar
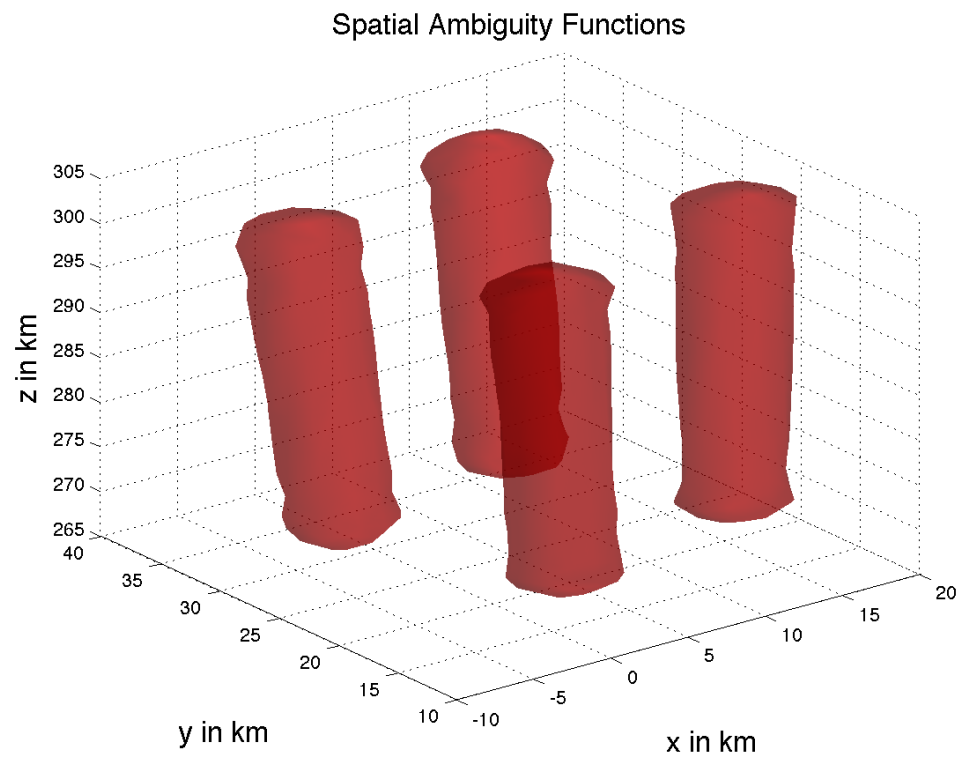
Figure 3. Full Spatial Ambiguity Function

Spatial Ambiguity Functions with Motion
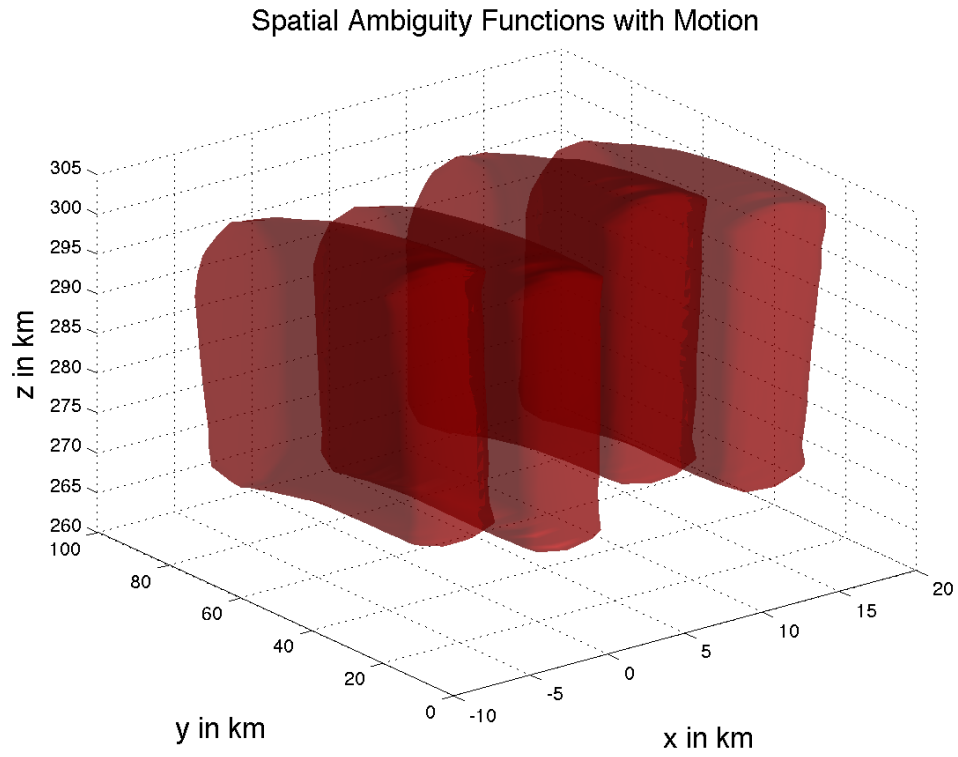
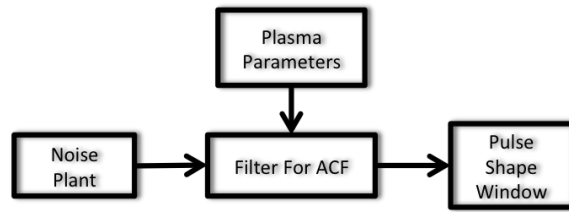**Figure 4.** Full Spatial Ambiguity Function With Motion

Figure 5. I/Q Simulator Diagram
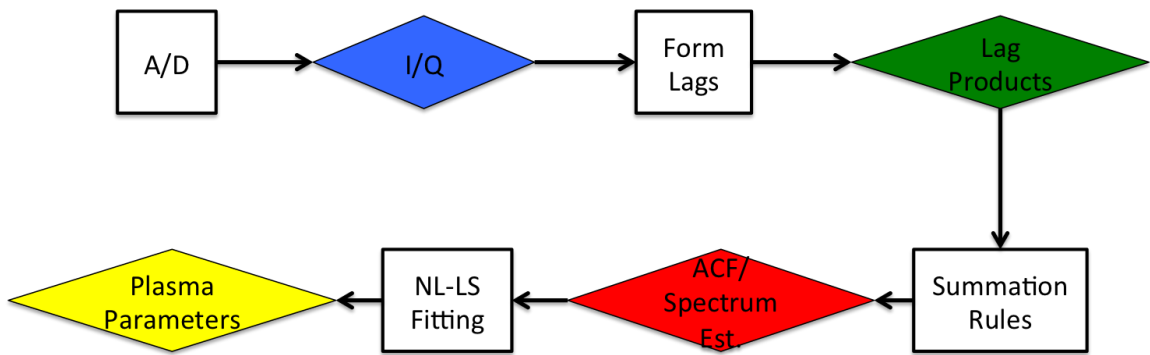
Figure 6. ISR Processing Chain.
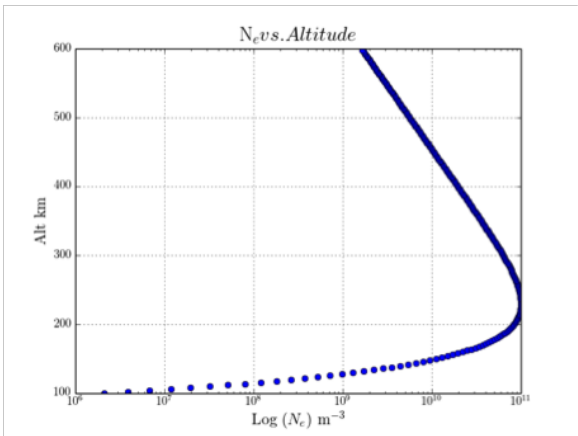
Figure 7. Electron density vs. altitude.
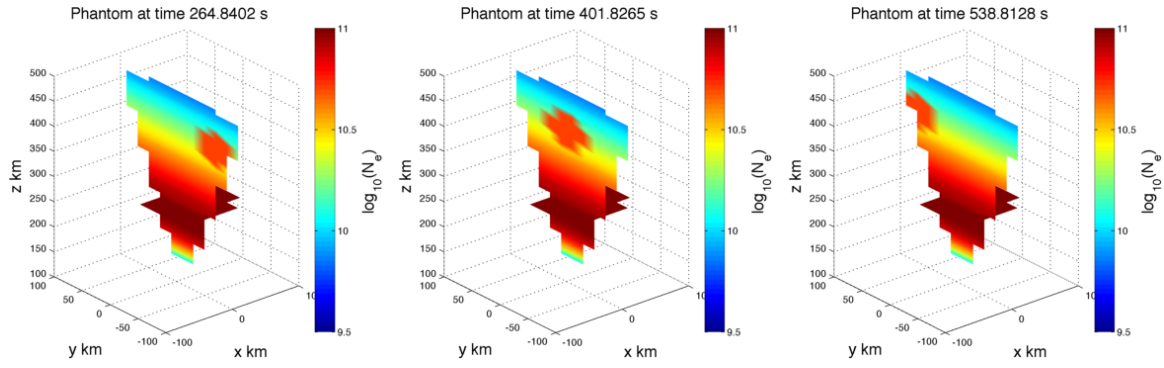
Figure 8.   Example images from phantom
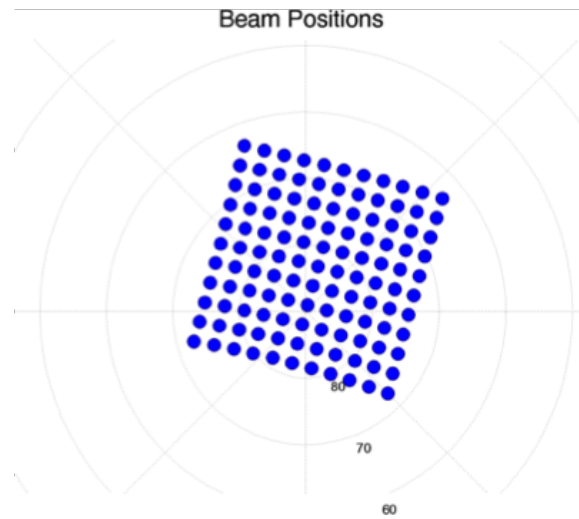
Figure 9.   Beam pattern
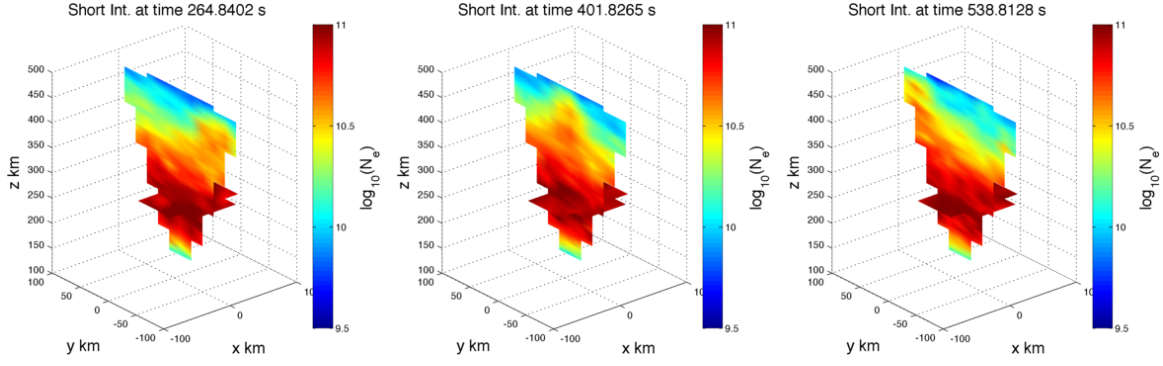
Figure 10.   Example images from variable data
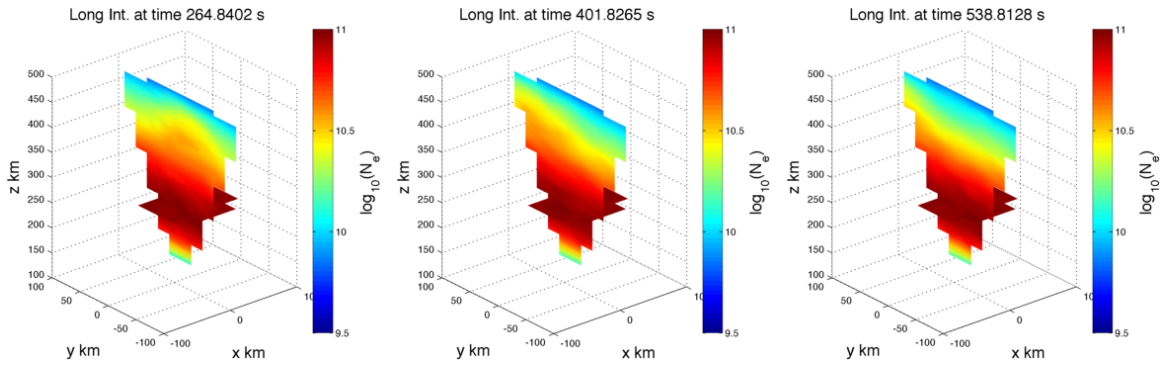
Figure 11.   Example images from blurred data
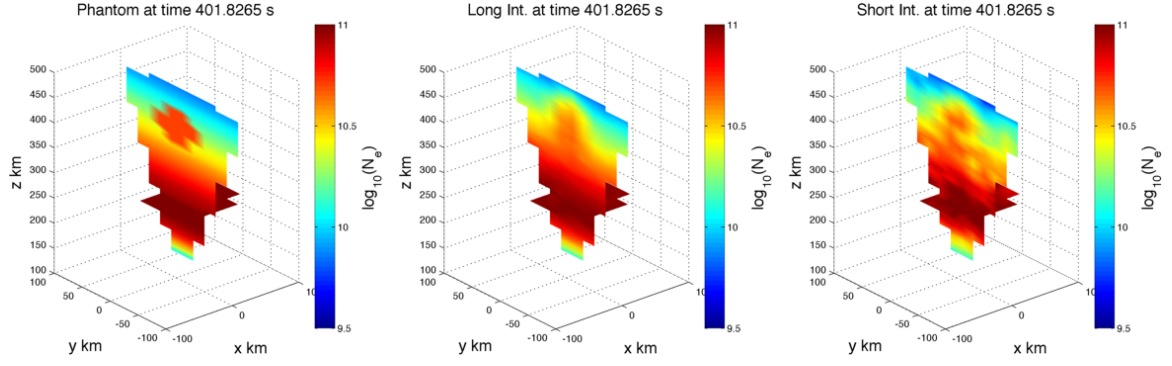
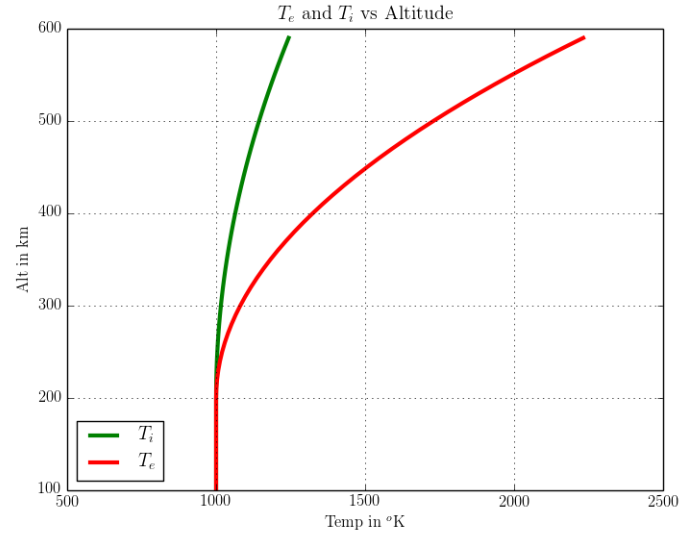**Figure 12.** Stationary phantom along with both types of reconstructions.

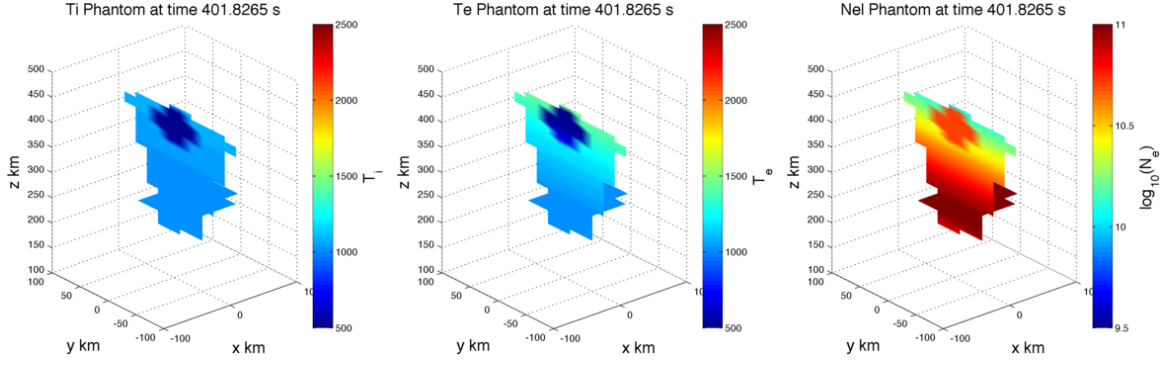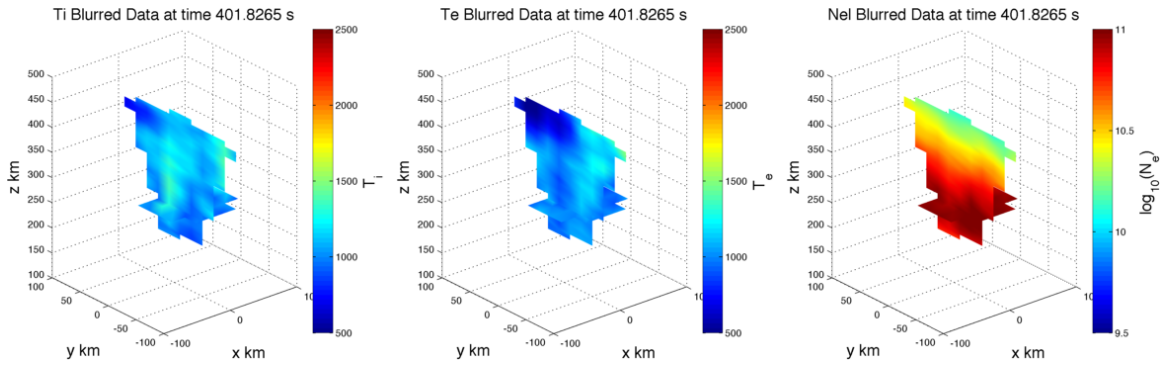**Figure 13.** Ion & electron temperature vs. height.

Figure 14. Phantom of parameters.

Figure 15. Blurred data after full fitting.